Impact of chaos and Brownian diffusion on irreversibility in Stokes flows

P. Sundararajan,[1] J. D. Kirtland,[2] D. L. Koch,[3] and A. D. Stroock[3,4,*]

[1]*Sibley School of Mechanical and Aerospace Engineering, Cornell University, Ithaca, New York 14853, USA*

[2]*Department of Physics and Astronomy, Alfred University, One Saxon Drive, Alfred, New York, 14802, USA*

[3]*Department of Chemical and Biomolecular Engineering, Cornell University, Ithaca, New York, 14853, USA*

[4]*Kavli Institute at Cornell for Nanoscale Science, Cornell University, Ithaca, New York, 14853, USA*

(Received 23 April 2012; revised manuscript received 9 August 2012; published 4 October 2012)

We study a reversal process in Stokes flows in the presence of weak diffusion in order to clarify the distinct effects that chaotic flows have on the loss of reversibility relative to nonchaotic flows. In all linear flows, including a representation of the baker's map, we show that the decay of reversibility presents universal properties. In nonlinear chaotic and nonchaotic flows, we show that this universality breaks down due to the distribution of strain rates. In the limit of infinitesimal diffusivity, we predict qualitatively distinct behavior in the chaotic case.

DOI: 10.1103/PhysRevE.86.046203 PACS number(s): 05.45.Ac, 05.70.Ln, 47.15.G−, 87.80.Qk

I. INTRODUCTION

A debate persists on whether dynamical chaos is the origin of irreversibility in the contexts of statistical mechanics [1,2] and transport phenomena [3,4]. On the one hand, running forward in time, chaotic systems, like the multibaker mapping, exhibit loss of time correlation and diffusive-like dynamics [5]. On the other hand, chaos is not intrinsically irreversible, in that, with infinite precision and in the absence of sources of random noise, chaotic trajectories will return to their original locations in phase space if the dynamics is reversed [6]. Experimental studies indicate that non-Brownian particles in oscillatory shear exhibit irreversibility and chaotic dynamics [3,4], but the relative importance of chaos and solid body contacts in preventing reversibility of the trajectories of the particles is not clear [7]. A challenge in defining the impact of chaos on irreversibility arises from the well-appreciated fact that chaotic flows accelerate the loss of reversibility in the presence of noise or finite precision relative to nonchaotic flows. In this paper, we adapt an analytical treatment of mixing (simultaneous convection and diffusion) put forth by Ranz [8] to scale the dynamics of diffusive tracers in a reversal experiment with respect to the characteristic rate of mixing. This approach elucidates a unity in the evolution of convective diffusive irreversibility in all linear flows and shows how this unity is disrupted by the presence of the distribution of strain rates in both chaotic and nonchaotic flows.

The reversal experiment that we consider is based on Heller's proposal [9,10] to use diffusive irreversibility in time-reversible Stokes flows as a means to separate solutes of distinct Brownian diffusivity from a mixture. Figure 1 illustrates his proposal for a mixture of two solutes: (i) stir the mixture [yellow region in Fig. 1(a)] until the distribution of the solute with higher diffusivity (green) has been largely homogenized into a carrier fluid [black region in Fig. 1(a)], (ii) "unstir" (reverse the flow) to completely undo the deformation [Fig. 1(c)], and (iii) collect the fluid from the original volume. The collected fluid will be partially purified of the tracers of higher diffusivity. We call this process separation by convective diffusive irreversibility, SCDI. In considering SCDI, Aref and Jones [11] defined return fraction R_f—the fraction of diffusive tracers that return to the original volume [Fig. 1(c)]—as a measure of reversibility. They showed that R_f decays faster in chaotic flows relative to nonchaotic flows for any amplitude of diffusivity and concluded that chaotic dynamics could, in this sense, enhance separation of diffusive solutes. Ottino [12] and others [13] have demonstrated experimentally this acceleration of the decay of reversibility by chaotic dynamics.

We now extend this investigation to ask further how chaotic flows impact the efficiency of SCDI relative to pure diffusion and nonchaotic flows. For this purpose, we define the maximum differential reversibility:

$$\phi(D_{\text{high}}, D_{\text{low}}) = \max\left(\frac{R_f(t_{\text{stir}}, D_{\text{low}})}{R_f(t_{\text{stir}}, D_{\text{high}})}\right)_{\forall t_{\text{stir}}}. \qquad (1)$$

This function is the maximum ratio of return fractions of tracers of distinct diffusivities D_{high} and D_{low} with respect to stirring time. This differential reversibility measures the sensitivity of reversal to differences in diffusive noise (a higher value of φ indicates greater sensitivity) and can serve as a figure of merit for its efficiency for SCDI; φ also provides a rate independent observable with which to compare the reversal process in the presence and absence of chaos.

II. RANZ MODEL

We first consider SCDI in three simple cases—(i) no flow such that the tracers evolve by pure diffusion; (ii) pure extensional flow such that the fluid undergoes deformation at an exponential rate; and (iii) simple shear flow such that the fluid undergoes deformation at an algebraic rate. Pure extension and simple shear are linear flows [14]. The work of Ranz [8] indicates that, for weak diffusion, mixing of a periodic array of bands of solute in linear flows [Fig. 2(a)] can capture mixing in the more general nonlinear flows because (1) the folding by a general flow typically results in an approximate spatial periodicity (λ) in the concentration field over short distances, and (2) the flow is approximately linear over short distances. In the case of pure extension, the evolution of these periodic strands represents mixing by the baker's transformation, a canonical model of chaotic

*ads10@cornell.edu

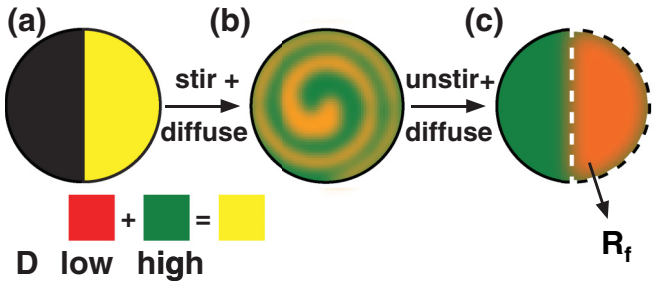

FIG. 1. (Color online) Schematic representation of separation by convective diffusive irreversibility (SCDI). Concentration profiles of a one-to-one mixture (yellow) of two solutes of different diffusivities (green = high diffusivity, red = low diffusivity) (a)–(c) State of mixture, (a) initially segregated from miscible carrier fluid (black) before stirring, (b) after stirring in a Stokes flow, and (c) after reversing the flow ("unstirring"). The white dashed line in (c) represents the original volume occupied by the mixture in which return fraction R_f is evaluated. High diffusivity solute is distributed uniformly over the domain in (c).

dynamics [15]. These strands, when observed in the local frame of reference (x',y') [Fig. 2(a), in which we translate and rotate with the strand] experience an effective rate of extension along y' of $\alpha(t,\dot\gamma) = -d\ln[s(t)/s(0)]/dt$ where $s(t)$ is the width of the strand at time t and $\dot\gamma$ is the actual strain rate in the flow. For simple shear flow, $\alpha = \dot\gamma t/[1+(\dot\gamma t)^2]$ and for extensional flow, $\alpha = \dot\gamma$. In this local frame (x',y'), the convection diffusion equation has the form

$$\frac{\partial c}{\partial t} - \alpha x'\frac{\partial c}{\partial x'} = D\frac{\partial^2 c}{\partial x'^2}. \tag{2}$$

We nondimensionalize time and position using the Ranz transformation:

$$\xi = x'/s(t) \text{ and } \tau = \int_0^t D dt'/s(t')^2. \tag{3}$$

The mixing time for extension τ_{ext}, simple shear τ_{ss}, and pure diffusion τ_d are

$$\tau_{\text{ext}} = \frac{D[\exp(2\dot\gamma t)-1]}{2\dot\gamma s_0^2}, \quad \tau_{ss} = \frac{D[\dot\gamma t + (\dot\gamma t)^3/3]}{\dot\gamma s_0^2},$$
$$\text{and} \quad \tau_d = \frac{Dt}{s_0^2}. \tag{4}$$

Physically, the mixing time τ represents the time required for a distribution of solute undergoing pure diffusion to reach the same state as the distribution would in the flow under consideration after a dimensional time t. The nondimensionalization in Eq. (3) reduces the convection-diffusion equation (2) to a transient diffusion equation:

$$\frac{\partial c}{\partial \tau} = \frac{\partial^2 c}{\partial \xi^2}. \tag{5}$$

The transformation to Eq. (5) indicates that the full dynamics of convection diffusion in linear flows can be captured by a purely diffusive process in the $\xi\tau$ domain with a nondimensional diffusivity of 1.

We can treat SCDI in these flows in a simple manner: using Eq. (5), we model the stirring phase by tracking the evolution

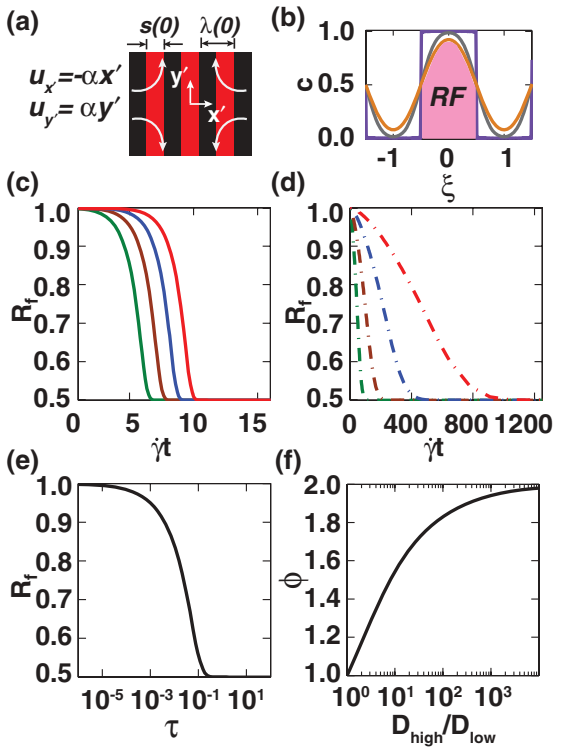

FIG. 2. (Color online) SCDI in linear flows. (a) Initial concentration distribution of a diffusive solute (red) in the frame of reference of the strand (x',y'). (b) Concentration profile $c(\xi,\tau)$ predicted by the Ranz model [Eq. (5)] initially ($\tau = 0$; violet curve), after stirring, ($\tau_{\text{stir}} = 0.02$; gray curve), and after unstirring ($\tau_{\text{unstir}} = 0.04$; orange curve). Return fraction R_f is defined as the area of shaded region. (c),(d) Decay of R_f for (c) extension (solid lines) and (d) simple shear (dash-dot lines) as a function of total strain, $\dot\gamma t$, for four different diffusivities [from left to right, 5.7×10^{-7} (green), 5.7×10^{-8} (brown), 5.7×10^{-9} (blue), 5.7×10^{-10} (red)]. (e) The master return curve $R_f(\tau_{\text{stir}})$ for all linear flows and pure diffusion. (f) The master curve of maximum differential reversibility, φ [Eq. (1)] for all linear flows plotted as a function of the ratio of diffusivities.

of the initial distribution, $c(\xi,\tau=0)$ for $\tau_{\text{stir}}(\dot\gamma t_{\text{stir}}, D)$, and the unstirring phase by tracking the evolution of the stirred distribution, $c(\xi,\tau_{\text{stir}})$, for an additional $\tau_{\text{unstir}}(\dot\gamma_{\text{unstir}} t_{\text{unstir}}, D)$. Using the conditions for complete unstirring, $t_{\text{stir}} = t_{\text{unstir}}$, and $\dot\gamma_{\text{unstir}} = -\dot\gamma$, we find that $\alpha(t_{\text{unstir}},\dot\gamma_{\text{unstir}}) = \alpha(t_{\text{stir}},-\dot\gamma) = -\alpha(t_{\text{stir}},\dot\gamma)$. Upon integrating Eq. (3), we find that $\tau_{\text{stir}} = \tau_{\text{unstir}}$. Hence the final distribution after stirring and unstirring is simply $c(\xi,2\tau_{\text{stir}})$. Figure 2(b) shows analytical solutions of Eq. (5) during the evolution of the initial square wave distribution. We evaluate $R_f(\tau_{\text{stir}})$ in the $\xi\tau$ domain as the ratio of the integrated concentration $c(\xi,2\tau_{\text{stir}})$ [shaded area in Fig. 2(b)] within the interval $(-0.5 \leqslant \xi \leqslant 0.5)$ to the integrated initial concentration $c(\xi,\tau=0)$ within the same interval. Further, $\varphi(D_{\text{high}},D_{\text{low}})$ can be evaluated from R_f with Eq. (1). Given the same initial condition and governing equation, the solutions and measures of reversibility are the same for all linear flows. Thus, using the Ranz transformation [Eq. (3)], we elucidate a unity in the decay of reversibility R_f and of the maximum differential reversibility $\varphi(D_{\text{high}},D_{\text{low}})$ in all convection-diffusion processes that are governed by Eq. (5).

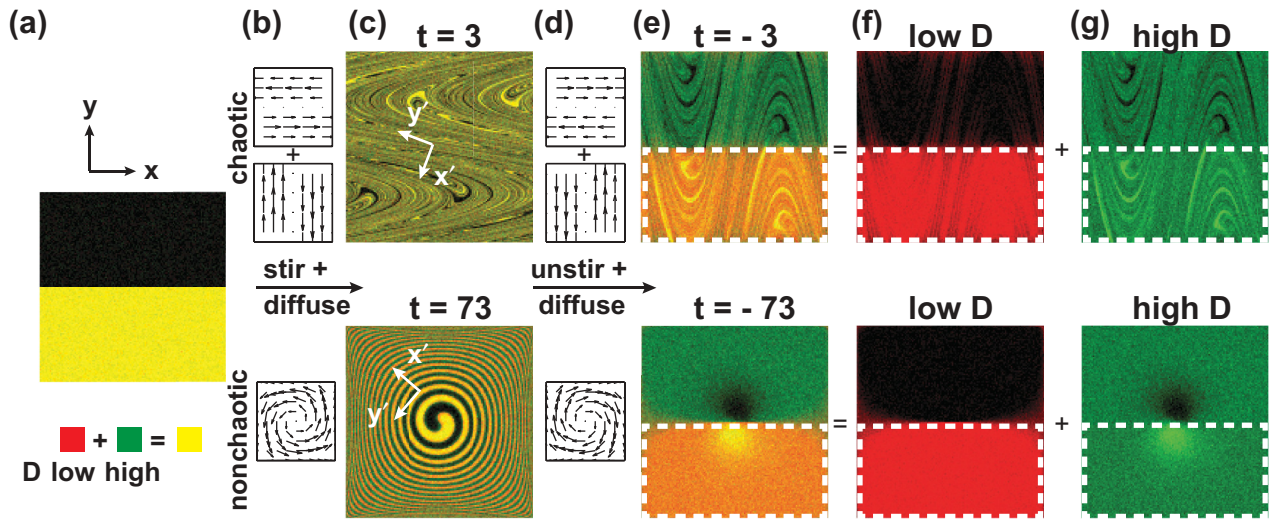

FIG. 3. (Color online) SCDI in nonlinear Stokes flows. Evolution of concentration profiles of a one-to-one mixture of two tracers of different diffusivities $D_{\text{high}} = 5.7 \times 10^{-7}$ (green) and $D_{\text{low}} = 5.7 \times 10^{-10}$ (red), (diffusion is nondimensionalized by $[H^2/T_{\text{cyc}}]$, where H is the height of the flow domain, T_{cyc} is the time period of the chaotic flow) in the chaotic (first row) and the nonchaotic (second row) flows. (a) Initial concentration profile with mixture in the lower half of the domain. (b) Schematic representation of the velocity fields used for stirring. (c) Concentration profile after stirring for t cycles ($t = 3$ for chaotic, $t = 73$ for nonchaotic) equivalent to the same mixing time τ of 0.24 and 0.000 24 for the two diffusivities in both flows. (d) Velocity fields used for unstirring. (e) Concentration profiles after unstirring for the t cycles. The white dashed line indicates the region where the solutes were present initially in (a). (f),(g) Individual concentration profiles after unstirring of (f) low diffusivity solute and (g) the high diffusivity solute. These distributions in (f) and (g) add up to give (e).

To appreciate the impact of the Ranz transformation, Figs. 2(c) and 2(d) show the rapid decay of return fraction as a function of total strain $\dot{\gamma}t$ in an extensional flow relative to that in a simple shear as observed by Aref and Jones [11]. Transforming to the τ domain in Fig. 2(e) [using Eq. (4)], the decay of R_f collapses into a single master return curve and this collapse results in a single master curve for differential reversibility [Fig. 2(f)]. We conclude that the exponential separation and the resulting sensitivity to noise in chaotic flows accelerate the decay of reversibility, but do not, on their own, disrupt the universality observed with the Ranz transformation or change differential reversibility relative to other linear flows.

III. NUMERICAL SIMULATION

We will now study SCDI in nonlinear velocity fields using the chaotic sine flow [16] and the nonchaotic steady Taylor-Green vortex flow [17] as examples (Fig. 3). In the chaotic case [Fig. 3(b), first row], the flow switches between two orthogonal sine flows with a period $T_{\text{cyc}} \equiv 1$ as given in Eqs. (6) and (7); in the nonchaotic case [Fig. 3(b), second row], the two sine flows operate continuously as given in Eq. (8),

$$\begin{aligned} u_x &= 1.75\sin(2\pi x); \quad u_y = 0; \\ nT_{\text{cyc}} &\leqslant t < 0.5(2n+1)T_{\text{cyc}}; \quad n = 0,1,2\ldots, \end{aligned} \tag{6}$$

$$\begin{aligned} u_x &= 0; \quad u_y = 1.75\sin(2\pi y); \\ 0.5(2n+1)T_{\text{cyc}} &\leqslant t < (n+1)T_{\text{cyc}}, \end{aligned} \tag{7}$$

$$\begin{aligned} u_x &= 0.6125\sin(\pi x)\cos(\pi y); \\ u_y &= 0.6125\sin(\pi y)\cos(\pi x). \end{aligned} \tag{8}$$

The flows evolve forward [stirring, Fig. 3(b)] for a time t (number of cycles for chaotic case) and then backward [unstirring, Fig. 3(d)] for the same time t. We note that this chaotic sine flow does not contain any nonchaotic islands. We simulate the evolution of the concentration profiles of a mixture of solutes of different diffusivities [Fig. 3(a)] with Lagrangian diffusive particle tracking as shown in Fig. 3. Briefly, the Lagrangian diffusive particle tracking method involves the following [18]: (a) populate the domain [Fig. 3(a)] using 10^6 particles randomly; (b) track the positions of the particles $\vec{x}$ in the chaotic and nonchaotic flows by solving for the particle trajectories $\frac{d\vec{x}}{dt} = \vec{u} + \vec{B}(t)$, where $\vec{u}$ is the velocity [as shown in Figs. 3(b) and 3(d)], and $\vec{B}(t)$ is the stochastic contribution to the velocity that represents diffusion; (c) obtain the concentration profiles [Figs. 3(c) and 3(e)–3(g)] by binning particle positions at chosen times.

IV. RESULTS AND DISCUSSION

A. Comparison with the Ranz model

In Figs. 4(a) and 4(b), we plot $R_f(\dot{\gamma}t, D)$ calculated with respect to the original volume bounded by the dashed white lines in Fig. 3(e) for each flow. Noting the similarity in $R_f(\dot{\gamma}t, D)$ in Figs. 4(a) and 4(b) (chaotic and nonchaotic flows) and Figs. 2(c) and 2(d) (extension and simple shear), we plot R_f as a function of the mixing time τ. For this purpose, we use $\tau_{\langle\dot{\gamma}\rangle}$ defined for linear flows in Eq. (4) (τ_{ext} for chaotic and τ_{ss} for nonchaotic flows, with two parameters, the mean strain rate $\langle\dot{\gamma}\rangle$ that we calculate independently and the initial strand thickness s_0 as an adjustable fitting parameter). Figure 4(c) shows that $R_f(\tau_{\langle\dot{\gamma}\rangle})$ appears to collapse for each class of flow for a range of diffusivities ($D = 5.7 \times 10^{-7} - 5.7 \times 10^{-10}$),

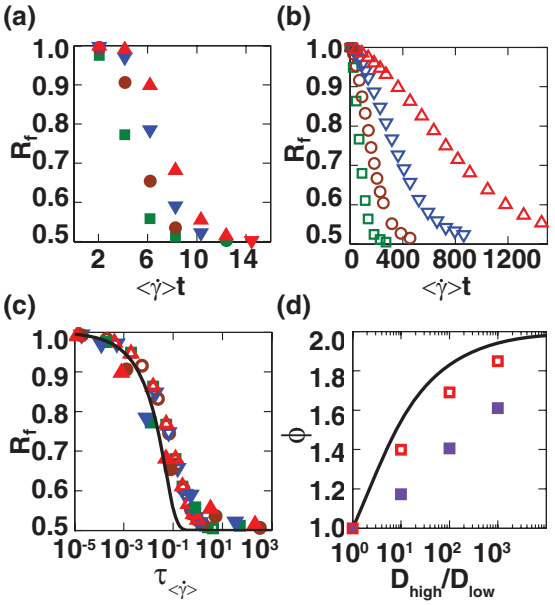

FIG. 4. (Color online) Characteristics of SCDI in nonlinear Stokes flows. (a),(b) R_f as a function of total strain (the mean strain rate $\langle\dot\gamma\rangle$ is 2.07 for the chaotic flow and 2.275 for the nonchaotic flow) for (a) the chaotic flow [$D = 5.7 \times 10^{-7}$ (■), 5.7×10^{-8} (●), 5.7×10^{-9} (▼), 5.7×10^{-10} (▲)] and (b) the nonchaotic flow [$D = 5.7 \times 10^{-7}$ (□), 5.7×10^{-8} (○), 5.7×10^{-9} (▽), 5.7×10^{-10} (△)]. (c) R_f as a function of mixing time $\tau_{\langle\dot\gamma\rangle}$ [with mean strain rates as in (b) and adjusted strand widths $s_0 = 0.375$ H for the chaotic ($r^2 > 0.99$) and 1.25 H for the nonchaotic flow ($r^2 > 0.99$)]. (d) Maximum differential reversibility φ as a function of the ratio of diffusivities for pure diffusive case [black line, same as Fig. 2(e)], chaotic flow (■), and nonchaotic flow (□).

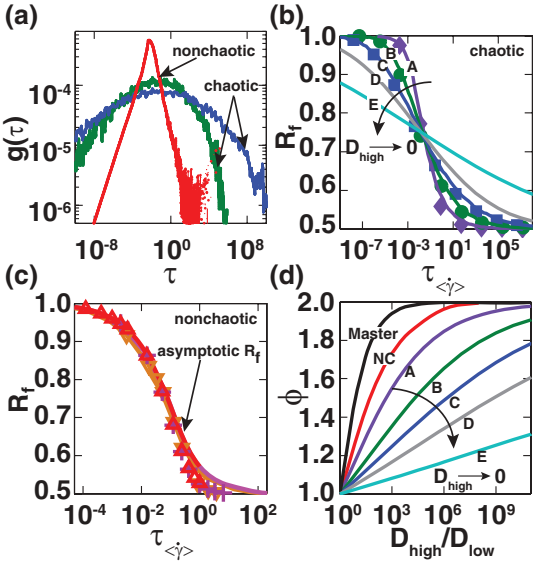

FIG. 5. (Color online) SCDI in the limit of infinitesimal diffusion using the modified Ranz model. (a) Mixing time distribution $g(\tau)$ in the chaotic flow for two diffusive solutes [$D = 5.7 \times 10^{-16}$ (●), $D = 5.7 \times 10^{-31}$ (●)] and in the nonchaotic flow for a diffusive solute [$D = 5.7 \times 10^{-16}$ (●)], for $\tau_{\langle\dot\gamma\rangle} = 0.024$. (b), (c) Return fraction R_f obtained from numerical simulation as a function of mixing time $\tau_{\langle\dot\gamma\rangle}$ for (b) the chaotic flow [diffusivities 5.7×10^{-7} (♦), 5.7×10^{-16} (●), and 5.7×10^{-31} (■)], and (c) the nonchaotic flow [5.7×10^{-4} (▽), 5.7×10^{-7} (+), 5.7×10^{-10} (△)]. Comparison with the return fraction based on modified Ranz model $R_{\mathrm{fMR}}(\tau_{\langle\dot\gamma\rangle})$ is shown using solid lines of the corresponding color for each diffusivity and flow [s_0 values in Fig. 3(c)]. In addition, in (b), return fraction $R_{\mathrm{fMR}}(\tau_{\langle\dot\gamma\rangle})$ corresponding to diffusivities $D = 5.7 \times 10^{-65}$ (_; D) and $D = 5.7 \times 10^{-257}$ (_; E) are plotted indicating the trend in R_f as $D \to 0$. (d) Maximum differential reversibility φ as a function of ratio of the diffusivities. The master φ curve for pure diffusion (_; Master), the asymptotic φ curve for nonchaotic flow as predicted by the modified Ranz model (_; NC), and trends for the chaotic case for D_{high} of 5.7×10^{-7} (_; A), 5.7×10^{-16} (_; B), 5.7×10^{-31} (_; C), 5.7×10^{-65} (_; D) and 5.7×10^{-257} [_; E)] as predicted by the modified Ranz model.

but not onto the master return curve for linear flows [black line replotted from Fig. 2(e)]. We also find that the evolution of $\varphi(D_{\mathrm{high}}, D_{\mathrm{low}})$ in chaotic flows and that in nonchaotic flows are distinct from each other and from that in linear flows [Fig. 4(d)]. The universal behavior of R_f and φ observed for linear flows does not generalize to nonlinear flows. Interestingly, the maximum differential reversibility is the smallest for the chaotic case. This observation indicates that, while chaos accelerates the absolute rate of decay of reversibility due to diffusion, it reduces the sensitivity to differences in diffusivity for nonlinear flows.

B. Modified Ranz model

We search for the origin of the distinct evolution of reversibility in linear and nonlinear flows seen in Figs. 4(c) and 4(d) in the character of the nonlinear flows. Strands in nonlinear flows experience a distribution of local strain rates which lead to a distribution of local mixing times $g(\tau)$. We generate the distribution of Lagrangian strain rates as follows: We track the length r of 10^4 line elements (with initial length $r_0 \equiv 1$) in these nonlinear flows by solving $\frac{d\vec r}{dt} = \vec r \cdot \vec\nabla \vec u$ along the trajectory of the center of the line elements. The Lagrangian strain rate is extracted for each line element using its relation to growth of line element in an extensional flow, $\dot\gamma(t) = \frac{1}{t}\ln(\frac{r}{r_0})$ for chaotic flows, and in a simple shear flow, $\dot\gamma(t) = \frac{1}{t}[\sqrt{(\frac{r}{r_0})^2 - 1}]$ for nonchaotic flows. The distribution of strain rates at any time is extracted from the ensemble of Lagrangian strain rates at that time. Finally, using Eq. (4) (τ_{ext} for chaotic and τ_{ss} for nonchaotic flow), we calculate the distribution of mixing times $g(\tau)$. Figure 5(a) presents $g(\tau)$ for the chaotic and nonchaotic cases. We note that the width of $g(\tau)$ grows exponentially with decreasing diffusivity in the chaotic flow whereas $g(\tau)$ reaches an asymptotic form in the nonchaotic flow.

To account for the impact of the distribution of strain rates on the decay of reversibility, we propose a modified Ranz model wherein we compute the weighted average return fraction $R_{\mathrm{fMR}}(\tau_{\langle\dot\gamma\rangle}) = \int_0^\infty R_f(\tau)g(\tau)d\tau$. Figures 5(b) and 5(c) indicate that the modified Ranz model captures the observed decay of $R_f(\tau_{\langle\dot\gamma\rangle})$ for both flows over an extensive range of diffusivities. Thus, the modified Ranz model provides a unified treatment of both chaotic and nonchaotic flows. We note that return fraction in a chaotic flow with islands would decay faster

initially due to exponential stretching of the chaotic regions as predicted above, followed by slower diffusive decay due to the islands [19].

C. Distinction in the zero diffusivity limit

To understand if there is a fundamental distinction between chaotic and nonchaotic flows in the context of SCDI, we explore the evolution of return fraction in chaotic and nonchaotic flows using the modified Ranz model in the limit $D \to 0$. Exploration of this limit is motivated by the observation that, while R_{fMR} in nonchaotic flows has already reached an asymptotic curve (distinct from the master return curve of linear flows) for $D = 5.7 \times 10^{-10}$ [Fig. 5(c)], the dependence of R_{fMR} on $\tau_{\langle\dot{\gamma}\rangle}$ in chaotic flows becomes increasingly weak [Fig. 5(b)]. Based on our modified Ranz model, we can identify the origin of this distinction of the nonlinear chaotic flow in the persistent growth of the tails of $g(\tau)$; this growth arises from the strong exponential dependence of the local mixing time τ_{ext} on the strain of the fluid element. As a result of these tails, R_{fMR} of the global flow is the combined effect of many fluid elements that are fully mixed, many that are unmixed for any finite D, and a small fraction (vanishingly small in the limit $D \to 0$) with an intermediate state of mixing that is sensitive to the precise value of D. When this weak dependence R_{fMR} on $\tau_{\langle\dot{\gamma}\rangle}$ for chaotic flows is expressed in terms of differential reversibility [lines labeled A, B, C, D, E in Fig. 5(d)], the trend indicates that the efficiency of reversal becomes completely insensitive to differences in diffusivity (i.e., $\varphi \to 1$ as $D \to 0$). In comparison, the asymptotic form of the R_{fMR} curve for nonchaotic flows results in an asymptotic form of differential reversibility [red line labeled NC in Fig. 5(d); different from the master differential reversibility curve (black line labeled Master)] at finite values of diffusivity. Thus, in the limit of infinitesimal diffusion, the underlying chaotic dynamics leads to complete insensitivity to different levels of diffusion, in distinct contrast to the nonchaotic case.

V. CONCLUSION

We have shown that, beneath the dramatically different rates of decay of reversibility observed in chaotic and nonchaotic flows, there exists significant unity in the evolution: (i) all linear flows lead to a universal decay of reversibility (R_f) when viewed in an appropriately scaled time domain, and (ii) a simple analysis that accounts for the distribution of strain rates successfully captures the decay in both chaotic and nonchaotic, nonlinear flows. Interestingly though, in the limit of infinitesimal diffusion, our analysis predicts a qualitative distinction between chaotic and nonchaotic, nonlinear flows with respect to differential reversibility. We emphasize that the distinction in this asymptotic behavior arises due to the interplay of dynamics, the distribution of rates, and diffusion, and not due to chaos acting as an intrinsic source of irreversibility. Finally, we note that our study indicates that a baker's transformation (with a single rate of strain) would be the optimal flow with which to implement Heller's separation strategy with respect to both rate and efficiency.

ACKNOWLEDGMENTS

We thank Dr. S. Verbridge and Dr. E. Villermaux for valuable suggestions. We acknowledge support from the National Science Foundation (Grant No. CTS-0529042) and the Department of Energy (Grant No. DE-FG02-05ER46250).

[1] B. Misra, I. Prigogine, and M. Courbage, Proc. Natl. Acad. Sci. USA **76**, 3607 (1979).
[2] J. L. Lebowitz, Phys. Today **46**(9), 32 (1993).
[3] G. Drazer, J. Koplik, B. Khusid, and A. Acrivos, J. Fluid Mech. **460**, 307 (2002).
[4] D. J. Pine, J. P. Gollub, J. F. Brady, and A. M. Leshansky, Nature (London) **438**, 997 (2005).
[5] P. Gaspard, *Chaos, Scattering and Statistical Mechanics* (Cambridge University Press, New York, 1998), pp. 250–253.
[6] D. Levesque and L. Verlet, J. Stat. Phys. **72**, 519 (1993).
[7] L. Corte, P. M. Chaikin, J. P. Gollub, and D. J. Pine, Nat. Phys. **4**, 420 (2008).
[8] W. E. Ranz, Aiche J. **25**, 41 (1979).
[9] J. P. Heller, Am. J. Phys. **28**, 348 (1960).
[10] G. I. Taylor, *Illustrated Experiments in Fluid Mechanics* (MIT, Cambridge, MA 1972), pp. 47–54.
[11] H. Aref and S. W. Jones, Phys. Fluids A: Fluid Dyn. **1**, 470 (1989).
[12] J. M. Ottino, *The Kinematics of Mixing: Stretching, Chaos, and Transport* (Cambridge University Press, Cambridge, England, 1997), pp. 213–214.
[13] P. Dutta and R. Chevray, Exp. Therm. Fluid Sci. **11**, 1 (1995).
[14] G. L. Leal, *Laminar Flow and Convective Transport Processes: Scaling Principles and Asymptotic Analysis* (Butterworth-Heinemann, Stoneham, MA, 1992), pp. 77, 171–172.
[15] T. Tél, M. Gruiz, and K. Kulacsy, *Chaotic Dynamics: An Introduction Based on Classical Mechanics* (Cambridge University Press, Cambridge, England, 2006), pp. 262–263.
[16] M. M. Alvarez, F. J. Muzzio, S. Cerbelli, A. Adrover, and M. Giona, Phys. Rev. Lett. **81**, 3395 (1998).
[17] G. I. Taylor and A. E. Green, Proc. R. Soc. London A **158**, 0499 (1937).
[18] J. D. Kirtland, G. J. McGraw, and A. D. Stroock, Phys. Fluids **18**, 13 (2006).
[19] P. B. Rhines and W. R. Young, J. Fluid Mech. **133**, 133 (1983).